Advanced Composites and Hybrid Materials (2019) 2:777–789
https://doi.org/10.1007/s42114-019-00131-6

ORIGINAL RESEARCH

Tribological behavior of aluminum nanocomposites studied by application of response surface methodology

I. Manivannan[1] · S. Ranganathan[2] · S. Gopalakannan[3]

Received: 17 July 2019 / Revised: 16 October 2019 / Accepted: 4 December 2019 / Published online: 12 December 2019

Abstract

An aluminum Al-0.8Al_2O_3 and Al − 1.6Al_2O_3 nanocomposite was prepared by a novel ultrasonic assisted stir casting method. A three-level Box-Behnken design of experiment was developed using response surface methodology. Dry sliding wear tests were performed as per the experimental design using a pin-on disc setup at room temperature. Analysis of variance (ANOVA) was applied to investigate the influence of process parameters, viz., wt.% reinforcement, load and sliding distance, and their interactions on specific wear rate and coefficient of friction. Further, a mathematical model has been formulated by applying response surface method in order to estimate the tribology characteristics such as wear and COF of the nanocomposites. The specific wear rate and coefficient of friction are significantly influenced by % of Al_2O_3 and load. The wear test parameters were optimized for minimizing specific wear rate and COF using desirability function approach. A set of optimum parameters of combination for AMMNC was identified as Al_2O_3–1.1 wt.%; load, 34 N and sliding distance, 2931 m with specific wear rate, 1.06 g/N-m; and coefficient of friction, 0.305. The AFM image of Al6061–1.1Al_2O_3 nanocomposite at optimized condition confirms the improvement in the wear surface smoothness of the nanocomposite compared to Al6061.

Keywords Nanocomposite · Wear · AFM · RSM · Desirability

1 Introduction

Conventionally, aluminum alloys are extensively employed in the manufacture of components in aeronautics and automotive sector due to its low density, good corrosion resistance, high damping capacity, and formability [1–3]. But Al alloys in their pure form possess less wear resistance which limits their use in certain fields. However, reinforcing the matrix alloy with hard ceramic particles improves the wear resistance of aluminum. The friction and wear of AMCs depend on the reinforcement content, size, and type. The reinforcing particles can be a carbide, oxide, or nitride [4–6]. The reinforcement of aluminum oxide (Al_2O_3) particles in aluminum leads to their superior wear resistance combined with a low friction coefficient. The development of Al/Al_2O_3 nanocomposite is a novel material in the area of $AMMNC_S$ with improved mechanical and tribological properties [7, 8]. The use of these novel Al/Al_2O_3 nanocomposite materials can improve energy efficiency, safety, and reliability [9–14].

Wang et al. established a novel method for dispersion of nanoparticles in molten metal by combined solidification process with ultrasonic cavitation [15]. Ezatpour et al. have successfully prepared A7075/Al_2O_3 nanocomposites with alumina powder of 0.4, 0.8, and 1.2 wt% by stir casting method followed by extrusion. The hardness, tensile, and compression strength of nanocomposite significantly improved compared to matrix alloy Al7075 [16]. Kumar and Balasubramanian developed a numerical model using RSM to forecast the abrasive wear rate of AA7075-SiC composite. The influence of volume % in

✉ I. Manivannan
i.manivannan72@gmail.com

S. Ranganathan
ranganathan.s@gmrit.edu.in

S. Gopalakannan
gopalakannan75@gmail.com

[1] Department of Mechanical Engineering, Motilal Nehru Government polytechnic college, Puducherry 605 008, India

[2] Department of Mechanical Engineering, GMR Institute of Technology, (An Autonomous Institution, Affiliated to JNTU, Kakinada), GMR Nagar, Razam, Andhra Pradesh 532127, India

[3] Department of Mechanical Engineering, Adhiparasakthi Engineering College, Tamil Nadu, Melmaruvathur 603 319, India

reinforcement, reinforcement size, applied load, and sliding speed on the wear behavior of AA7075-SiC composite was analyzed, and it was inferred that the reinforcement size exerted the greatest effect on wear [17]. Basavarajappa et al. (2007) fabricated Al-SiC-Gr hybrid composites by liquid metallurgy route, and the results of dry sliding wear of the hybrid composite were compared with that of Al-SiC composite. Using Taguchi technique, a set of experimental data for optimization was developed in a controlled manner. He concluded that wear of Al-SiC composite and Al-SiC-Gr hybrid composites is greatly affected by the sliding distance [18]. Sahin (2010) developed Al-15 wt% SiC composite by powder metallurgy (PM) method and used analysis of variance (ANOVA) to examine the input parameters which affect the wear of the Al-15 wt% SiC composite. He stated that the abrasive wear is significantly affected by abrasive grain size followed by hardness [19]. Suresha and Sridhara (2010) developed Al-SiC-Gr hybrid composite by stir casting method and studied the tribological behavior under dry sliding condition. Design of experiment (DOE) technique was employed to study the influence of parameters like load, sliding distance, sliding speed, and % reinforcement. They concluded that load and sliding distance have positive effect on the wear of the hybrid composite [20]. In addition, various research work on the wear behavior of AMCs, and optimization has been done and reported [21–23].

However, the parametric studies on the dry sliding wear of AMMNCs are scarce. In this present work, an attempt is made to study the influence of process parameters, viz., load, sliding distance, % reinforcement, and their interactions on specific wear rate (SWR) and coefficient of friction (COF) of Al-Al_2O_3 nanocomposite by using RSM.

2 Materials and methods

2.1 Fabrication of Al6061-Al_2O_3 nanocomposites

Al6061-Al_2O_3 nanocomposite was fabricated by ultrasonic cavitation method by adding aluminum oxide (Al_2O_3) of 0.8 and 1.6% by weight basis. Figure 1 shows the ultrasonic cavitation assisted stir casting setup. For each casting, about 1 kg of Al6061 was first melted in the crucible to a temperature of 750 °C. Al_2O_3 nanoparticle was preheated to 800 °C for 1 h in a muffle furnace in order to improve the wettability [5]. When nano-Al_2O_3 were added in the matrix alloy melt, the viscosity of the Al6061 matrix alloy significantly increased. To improve the wettability of the nanoparticles, efficient ultrasonic treatment done in the melt pool and maintained casting temperature of 750 °C to ensure the flow ability inside the mold. The Al6061-Al_2O_3 nanocomposite was fabricated [6].

Fig. 1 (a) Experimental setup for fabricating nanocomposites

2.2 Characterizations of Al6061-Al_2O_3 nanocomposites

The mean particle size of the nano-Al_2O_3 particle purchased from US Research Nanomaterials, Inc., USA, was measured using Horiba SZ-100 particle analyzer. The particle size obtained by this process was measured as 60 nm. Figure 2 shows the distribution of particle size of nano-Al_2O_3 particle by particle analyzer in the form of the distribution curve.

A Carl Zeiss NTS GMBH, Germany (SUPRA 55), Field Emission Scanning Electron Microscope (FESEM) images were used for the assessment of the morphology of raw materials and casted nanocomposite materials. Figure 3(a) shows the SEM image of Al6061, Fig. 3(b) shows SEM image of nano-Al_2O_3, Fig. 3(c) shows SEM image of Al-0.8Al_2O_3 nanocomposite, and Fig. 3(d) shows SEM image of Al-1.6Al_2O_3 nanocomposite. The nano-Al_2O_3 are uniformly distributed with some microclusters in Al-0.8Al_2O_3 nanocomposite. Agglomerations of nano-Al_2O_3 particles are observed in Al-1.6Al_2O_3 nanocomposite. When the particles were wetted in the metal melt, the particles will tend to sink or float to the molten melt due to the density differences between the reinforcement particles and the matrix alloy melt, so that the dispersion of the ceramic particles is not uniform and particles have high tendency for agglomeration and clustering. Wettability and distribution of reinforcement particles become more difficult when the particle size decreases to the nanoscales. This is due to the increasing surface area and surface energy of nanoparticles which cause an increasing tendency for agglomeration of reinforcement particles.

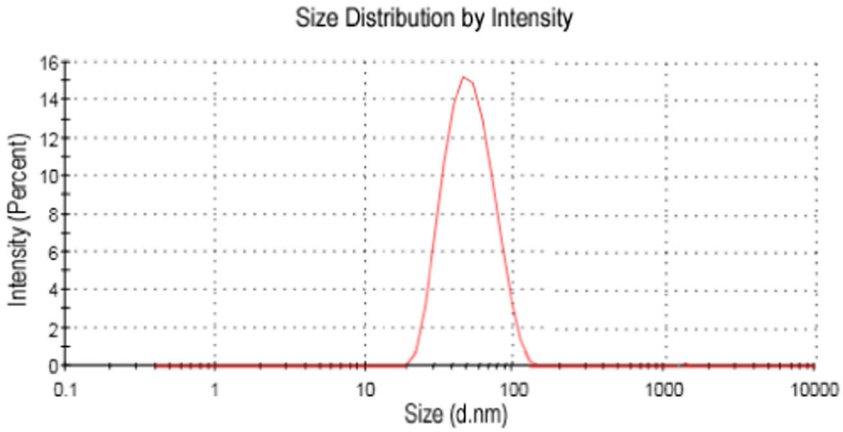

Fig. 2 Size distribution of nano-Al_2O_3 particle

Moreover, several structural defects such as porosity, particle clusters, oxide inclusions, and interfacial reactions arise from the unsatisfactory casting technology [7]. The scale bar for base material Al6061 is 20 μm. The scale bar for nano-Al_2O_3 is 200 nm to note down the nano-Al_2O_3 particle. The scale bar for Al606–0.8Al_2O_3 nanocomposite and Al6061–1.6Al_2O_3 nanocomposite is 1 μm which is in well agreement with the results of the various researchers S.A. Sajjadi et.al (2011) and HR Ezatpour et.al (2015) reported previously. The hardness of Al6061 is 55VHN, Al-0.8Al_2O_3 nanocomposite is 80VHN, and Al-1.6Al_2O_3 is 89VHN nanocomposite. There is a significant improvement in hardness of nanocomposites

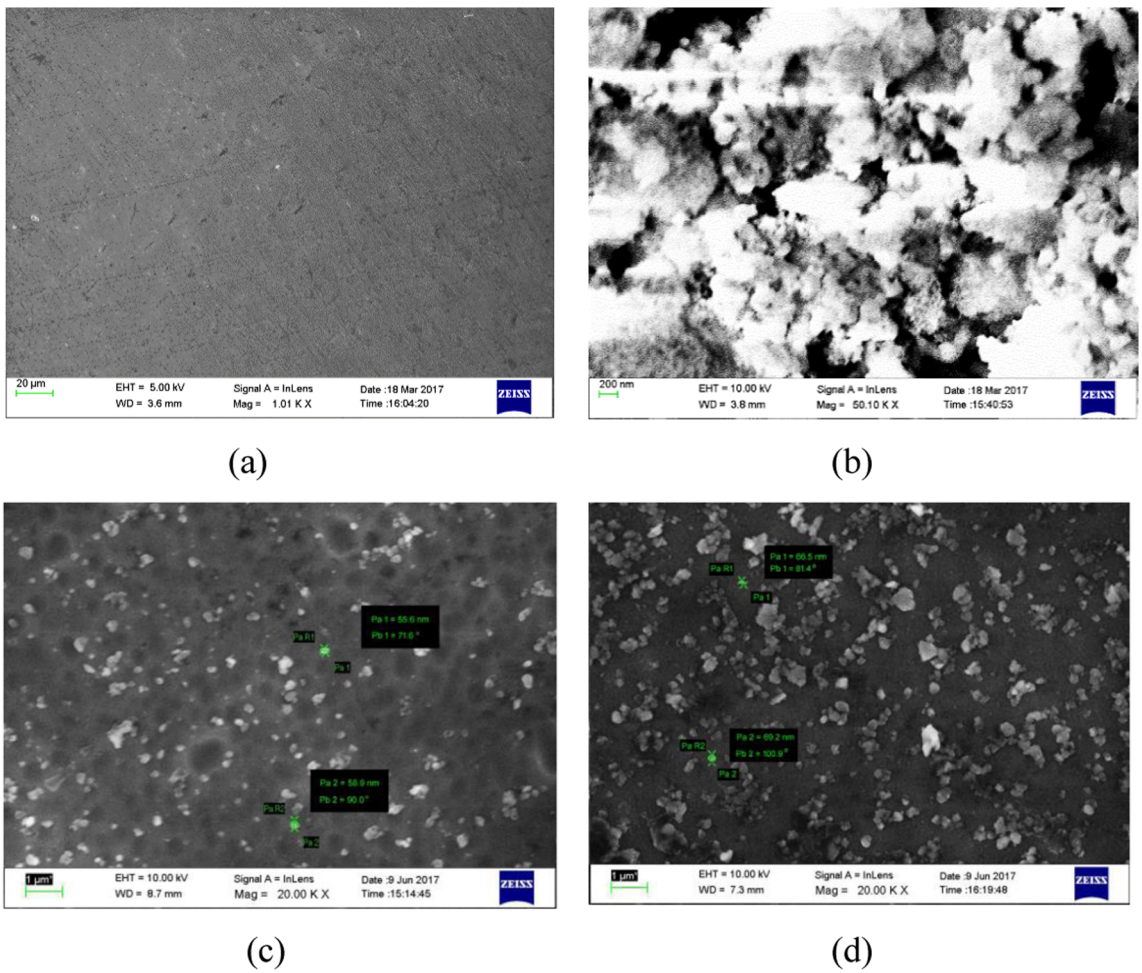

Fig. 3 (a) SEM of Al6061, (b) SEM of nano-Al_2O_3, (c) SEM of Al6061–0.8Al_2O_3 nanocomposite, (d) SEM of Al6061–1.6Al_2O_3 nanocomposite

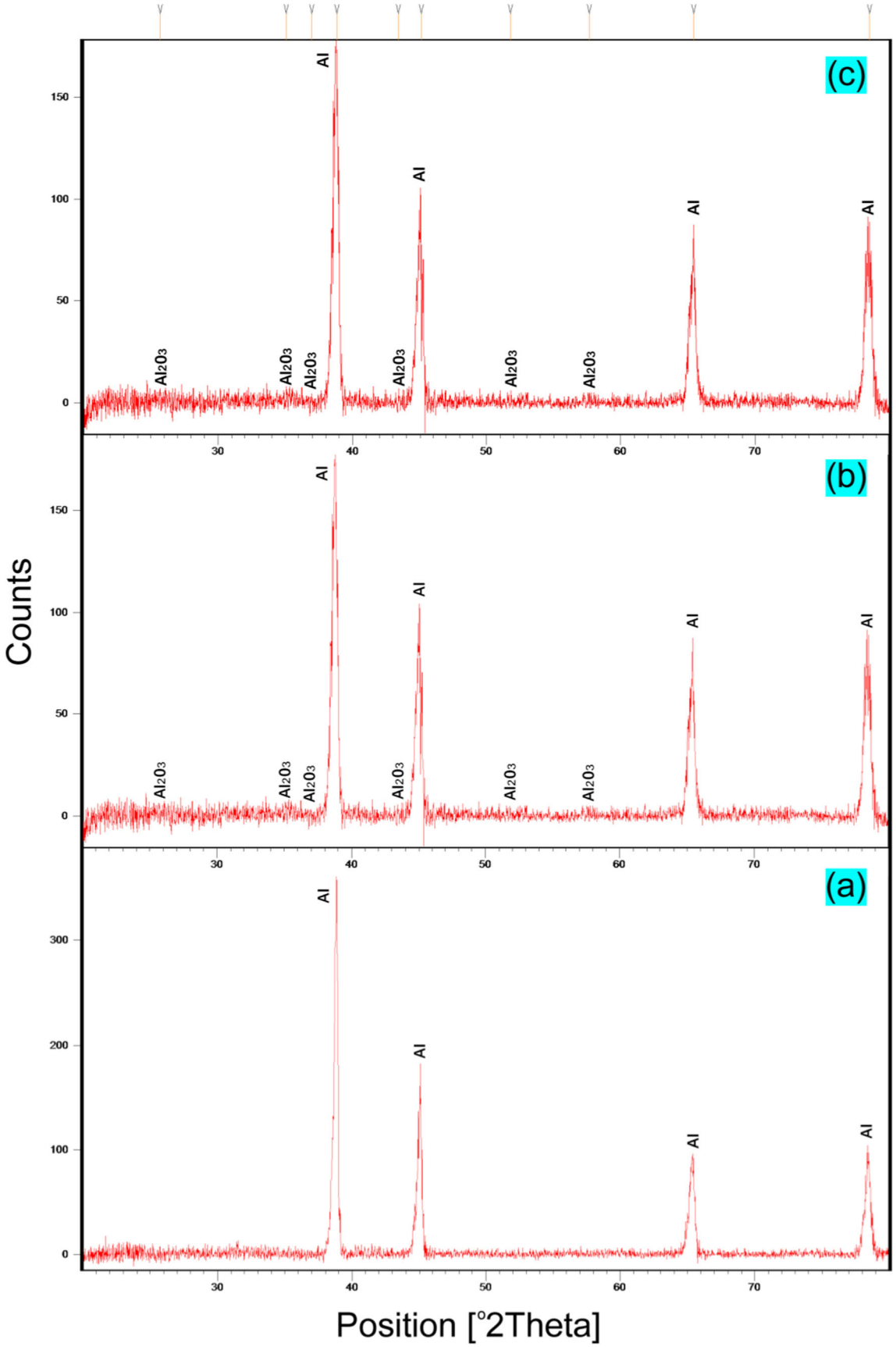

Fig. 4 (a) XRD of Al6061, (b) XRD of Al6061–0.8Al_2O_3 nanocomposite, (c) XRD of Al6061–1.6 Al_2O_3 nanocomposite

Table 1 Input levels of sliding wear parameters

Sl. No	Parameter	Notation	Unit	Level		
				–1	0	+1
1	wt.% of Al_2O_3	A	%	0	0.8	1.6
2	Sliding distance	B	m	1000	2000	3000
3	Load	C	N	20	30	40

compared to the Al6061.This is attributed to the presence of nano-Al_2O_3 in the matrix alloy which restricts the dislocation movement [4, 6].

X'Pert PRO (PANalytical) X-ray diffractometer with Cu Ka radiation at the voltage of 40 kV was used for carrying out XRD analysis with the current like 30 mA. Twenty data from 20° to 80° was collected by following continuous scan mode. The XRD results of Al6061, Al606–0.8Al_2O_3, and Al6061–1.6Al_2O_3 nanocomposites are shown in Fig. 4. The presence of aluminum and Al_2O_3 particles is confirmed by different peak intensities as shown in Fig. 4. The presence of major peaks indicates aluminum, and very minor peaks represent the Al_2O_3 particles. The peaks of Al_2O_3 nanocomposites seem weak because the weight fraction of Al_2O_3 (0.8 wt% i.e., 8 *g*, and 1.6 wt% i.e., 16 g in 1 kg of aluminum for a batch) is less than that of aluminum. It is also observed from Fig. 4 that there is no evidence of new phases (intermetallic compounds) which were attributed to no interfacial reactions and good dispersion of Al_2O_3 during casting process. Also it is clearly seen that the Al peaks marginally shift to higher angles as the weight % of the aluminum oxide is increased. The nanophase identification is in good agreement with Ravindran et al. (2013) and Li et al. (2018).

Table 2 Design factors and responses in coded form

Ex. No	Run	% of Al_2O_3	Sliding distance, m	Load (N)	Specific wear rate × 10–7 (g/N-m)	Coefficient of friction μ
1	13	0.8	2000	30	1.51	0.336
2	8	1.6	2000	40	1.36	0.311
3	2	1.6	1000	30	1.8	0.346
4	7	0	2000	40	3.53	0.65
5	12	0.8	3000	40	1.19	0.315
6	17	0.8	2000	30	1.51	0.336
7	15	0.8	2000	30	1.51	0.336
8	14	0.8	2000	30	1.51	0.336
9	1	0	1000	30	3.4	0.53
10	11	0.8	1000	40	1.6	0.338
11	9	0.8	1000	20	1.85	0.355
12	5	0	2000	20	2.16	0.5
13	16	0.8	2000	30	1.51	0.336
14	4	1.6	3000	30	1.35	0.319
15	6	1.6	2000	20	1.69	0.348
16	3	0	3000	30	2.38	0.57
17	10	0.8	3000	20	1.46	0.341

Table 3 ANOVA for response surface quadratic model of specific

Source	Sum of square	Degree of freedom	Mean square	*F*-value	*P* value
Model	6.99	9	0.78	15.08	0.0008
A-Al_2o_3	3.47	1	3.47	67.44	< 0.0001
B-sliding distance (m)	0.64	1	0.64	12.51	0.0095
C-load (N)	0.034	1	0.034	0.66	0.4444
AC	0.72	1	0.72	14.04	0.0072
A2	2.01	1	2.01	39.09	0.0004
Residual	0.48	12	0.04		
Lack of fit	0.48	8	0.06		
Pure error	0	4	0		
Cor total	7.35	16			

Standard deviation, 0.20; R^2, 0.9392; adjusted R^2, 0.9116; and predicted R^2, 0.7515

2.3 Wear test

The tribological studies were carried out on a computer integrated monitor (TR-20-PHM-M1 DUCOM) with an inbuilt load cell to measure the frictional force. For wear test, pins are machined to 10 mm diameter and 20 mm height. Disc surface of 25 mm diameter is maintained as sliding path. The tribo-testing was carried out at three different normal loads (20 N, 30 N, and 40 N). The

Table 4 ANOVA for response surface quadratic model of coefficient

Source	Sum of squares	Degree of freedom	Mean square	*F*-value	*P* value
Model	0.17	3	0.056	124.63	< 0.0001
A-%Al_2o_3	0.11	1	0.11	239.46	< 0.0001
AC	8.74E-03	1	8.74E-03	19.53	0.0007
A2	0.051	1	0.051	114.89	< 0.0001
Residual	5.82E-03	13	4.48E-04		
Lack of fit	5.82E-03	9	6.47E-04		
Pure error	0	4	0		
Cor total	0.17	16			

Standard deviation, 0.021; R^2, 0.9664; adjusted R^2, 0.9586; and predicted R^2, 0.8977

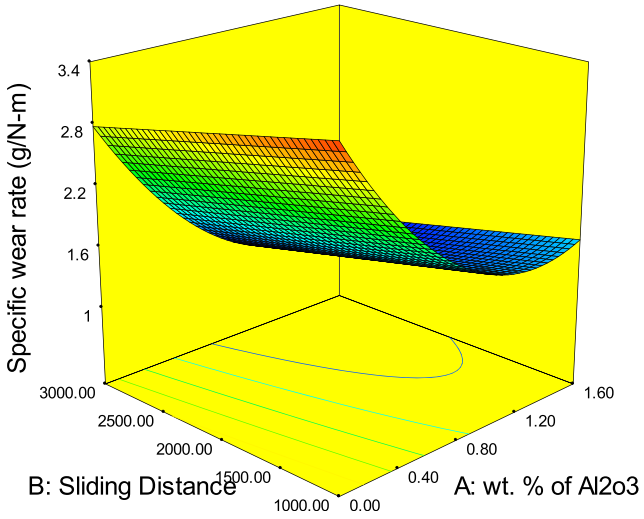

Fig. 5 Interaction plot for specific wear rate 3D plot

sliding distance of 1000 m, 2000 m, and 3000 m and sliding velocity of 0.5 m/s were used. The COF is directly recorded by a computer system connected to the wear test machine. The wear test procedure followed according to ASTM G99 standard has been discussed in our earlier work [6]. The three-dimensional topography of worn surface was analyzed by XE 70, Park Systems, a Korean-made atomic force microscope (AFM).

3 Dry sliding wear studies by RSM method

3.1 Experimental design

RSM is used to find the relation between a set of input parameters and its output response. Design Expert-16 software is used to design the experiment and to study the effect of input parameters on SWR and COF of aluminum nanocomposite. In this study, three factors with three levels as shown in Table. 1 are used. Reinforcement % of Al_2O_3, sliding distance, and load are the input factors considered in this study. Table. 2 shows the number of experiments to be conducted as per the experimental design matrix.

4 Results and discussion

4.1 Mathematical model for SWR and COF

For analysis of SWR and COF, the quadratic model suggested from the fit summary is statistically significant. ANOVA (Table 3 and Table 4) contains the results of the quadratic models. When the value of R^2 approaches unity, the difference between actual and predicted data is very less which means that the response model fits the actual data. Further, if adequate precision (AP) is greater than 4, the predicted value can be compared with the average prediction error at the design point. Signal to noise ratio discriminates the adequate model if the value is greater than 4. These developed models have higher R^2 and AP values. The values obtained are as follows: $R^2 = 0.9392$ and $AP = 18.290$ for SWR and $R^2 = 0.9664$ and $AP = 31.66$ for COF. Subsequently, these mathematical models developed for SWR and COF are considered to be significant. The lack of fit test must be insignificant. The insignificant terms are removed by backward elimination process to fit in to the quadratic models [24]. After backward elimination process, the response equations of SWR and COF of the final quadratic models are presented below.

$$\text{Specific wear rate (g/N–m)} = +1.52-0.66*A-0.28*B-0.42A*C+0.69*A*A$$

$$\text{Coefficient of friction}(\mu) = +0.34-0.12*A-0.048*A*C+0.12*A2$$

4.2 Effect of dry sliding parameters on SWR

The surface graph in Fig. 5 shows the influence of % of Al_2O_3 on SWR of Al6061-Al_2O_3 nanocomposites for the applied load of 20–40 N and sliding distance of 1000–3000 m. It is observed that when the applied load increased, the SWR decreased due to the development of mechanically mixed layer (MML layer). On comparing all the nanocomposites, when the Al_2O_3% is increased, SWR decreased up to 1.2% and increases for 1.6%. The

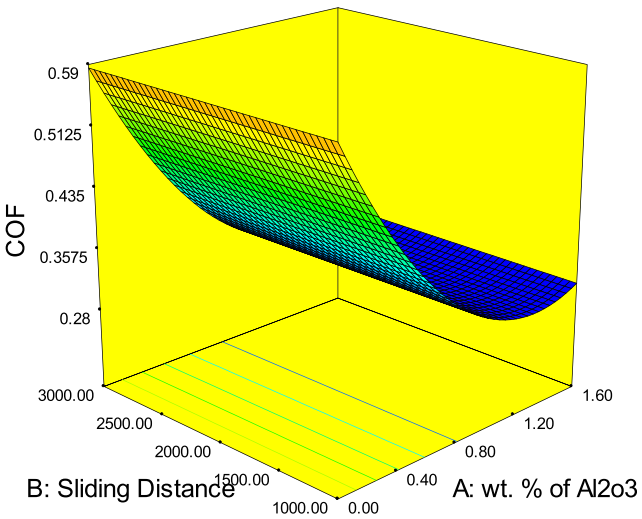

Fig. 6 Interaction plot for coefficient of friction 3D plot

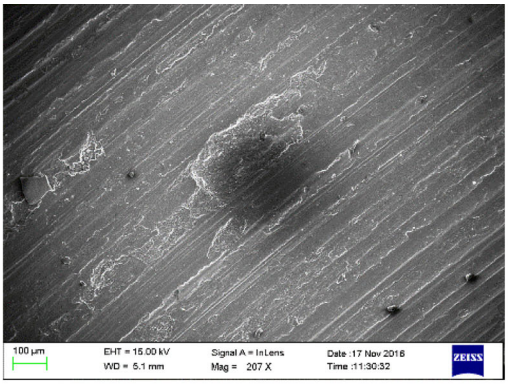

(a)

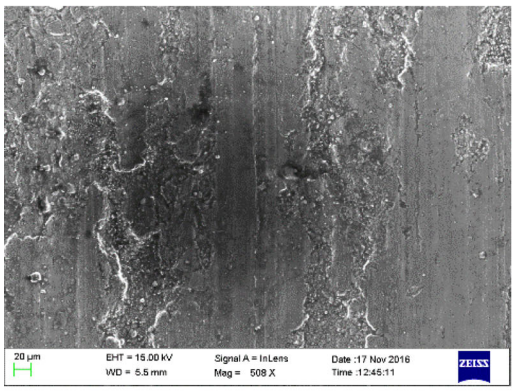

(b)

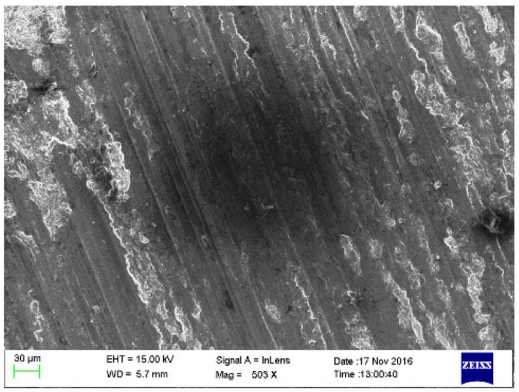

(c)

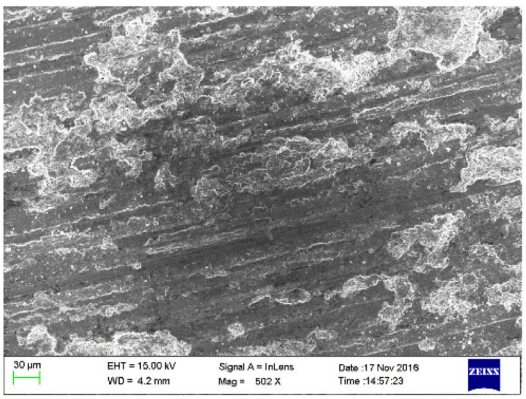

(d)

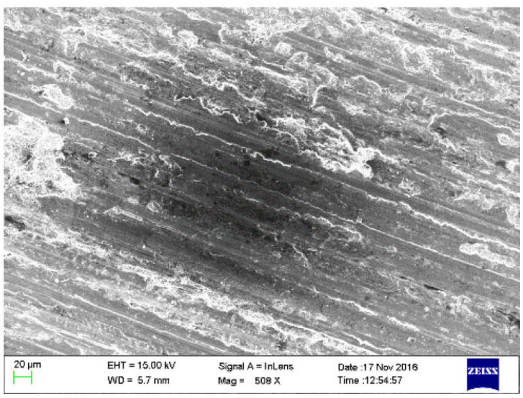

(e)

Fig. 7 SEM of worn surfaces of (a) Al6061 D-2000 m L-40 N, (b) Al-0.8 Al_2O_3 D-3000 L-20 N, (c) Al-0.8Al_2O_3 D-3000 L-40 N, (d) Al-1.6Al_2O_3 D-2000 L-20 N, (e) Al-1.6Al_2O_3 D-2000 L-40 N. *L* load, *D* sliding distance

increase in SWR is due to more agglomeration at 1.6% of Al_2O_3. For all applied load, the SWR decreased due to significant improvement in hardness of Al-Al_2O_3 nanocomposites. This is attributed to hard nano-Al_2O_3 particles on reinforcement with Al6061 matrix alloy that creates good interfacial bonding of the nanocomposite

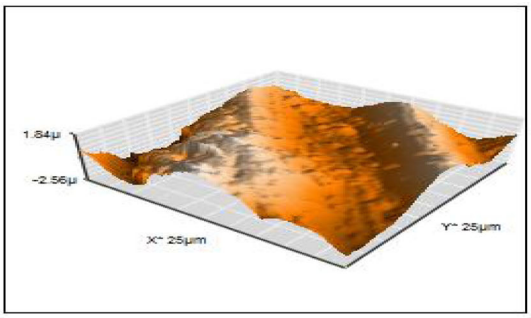

(a)

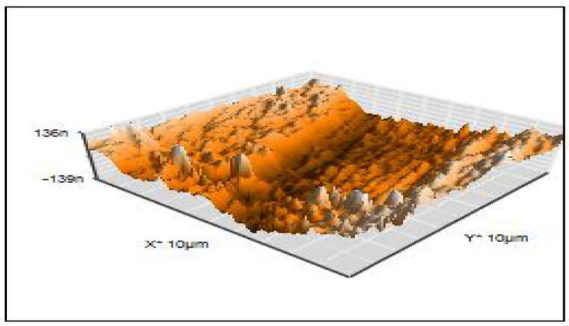

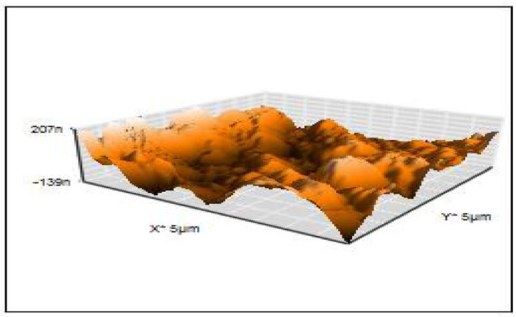

(b) (c)

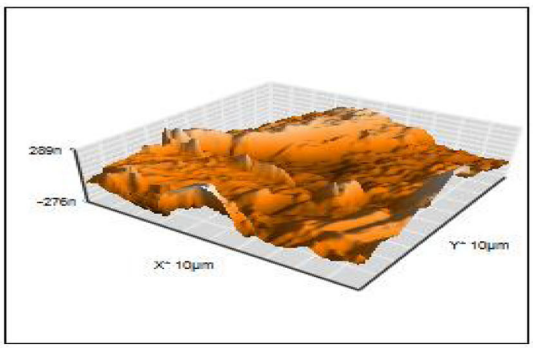

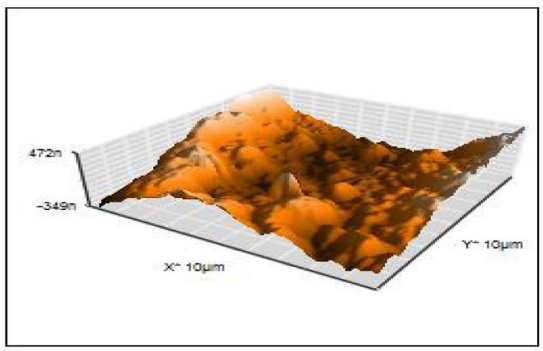

(d) (e)

Fig. 8 AFM (3D) of (a) Al6061 D-2000 m L-40 N, (b) Al-0.8Al_2O_3 D-3000 L-20 N, (c) Al-0.8 Al_2O_3 D-3000 L-40 N, (d) Al-1.6Al_2O_3 D-2000 L-20 N, (e) Al-1.6Al_2O_3 D-2000 L-40 N. *L* load, *D* sliding distance

which improves the mechanical properties hardness and strength. During sliding, the Al_2O_3 particles act as load bearers and protect the soft matrix alloy from wear. The wear trend of the present work is consistent with Mosleh-shirazi and Akhlaghi [4]. The SWR is significantly influenced by % Al_2O_3 followed by load.

4.3 Effect of dry sliding parameters on COF

Figure 6 shows the effect of load, sliding distance, and % of Al_2O_3 on COF of Al-Al_2O_3 nanocomposite. It is noted that COF decrease when load is increased from 20 to 40 N. Due to the formation of mechanically mixed layer

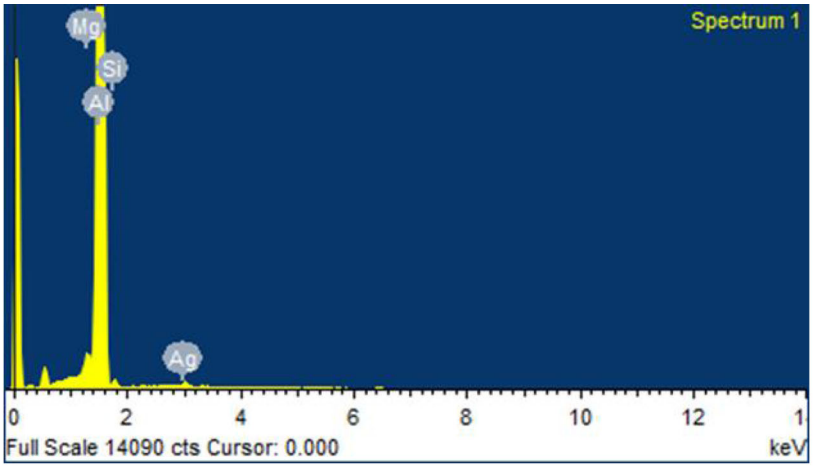

(a)

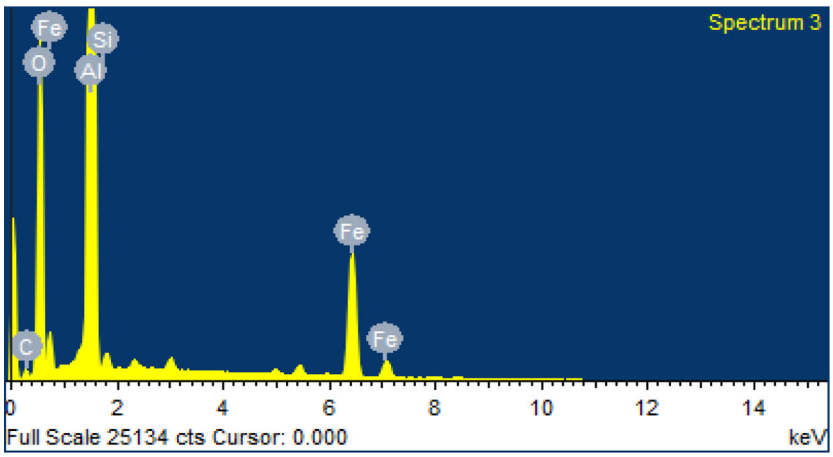

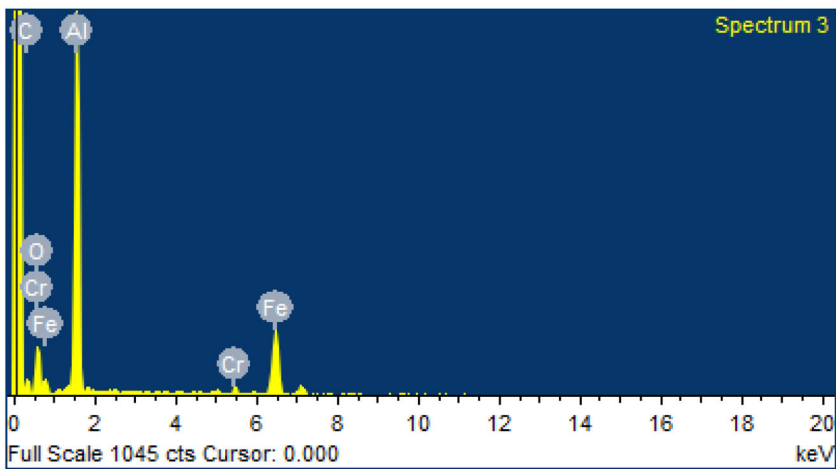

Fig. 9 EDS results of wear worn surface for various composites under 40 N load (a) Al6061, (b) Al6061–0.8Al_2O_3, (c) Al6061–1.6Al_2O_3

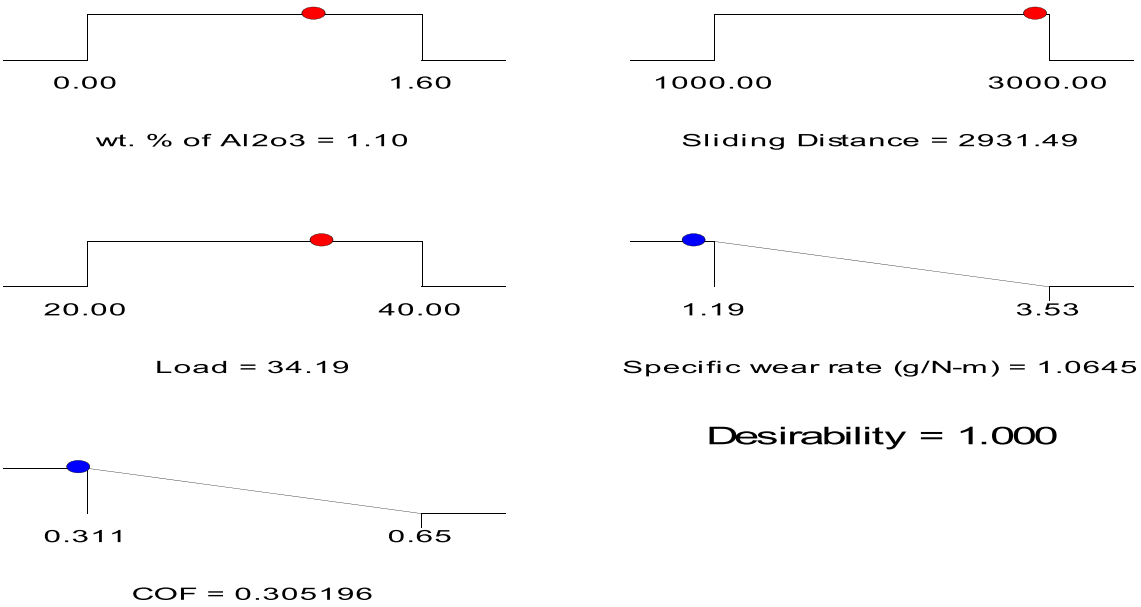

Fig. 10 Ramp function graph of desirability

in Al-Al_2O_3 nanocomposites at high load, friction between disc and pin get reduced resulting in lowered COF compared to Al6061 matrix alloy. The existence of a stable mechanically mixed layer at the point of contact is the key factor in reducing the COF of nanocomposite independent of sliding distance. The COF value decreases as the % of Al_2O_3 is increased up to 1.2%, but the COF increases beyond 1.2% of Al_2O_3. The COF is significantly influenced by % Al_2O_3 followed by load.

4.4 Worn surface analysis for various nanocomposites

The morphology of the wear surface of Al6061 matrix and Al606–0.8Al_2O_3 nanocomposite pin tested at load of 20 *N*–40 N is shown in Fig. 7(a–e). The SEM image provides valuable information about the wear mechanism of alloy and nanocomposite. On increasing the load to 40 N, abrasive wear decreases, and adhesive wear increases, which is clearly identified by big size wear debris as shown in Fig. 7(a). The

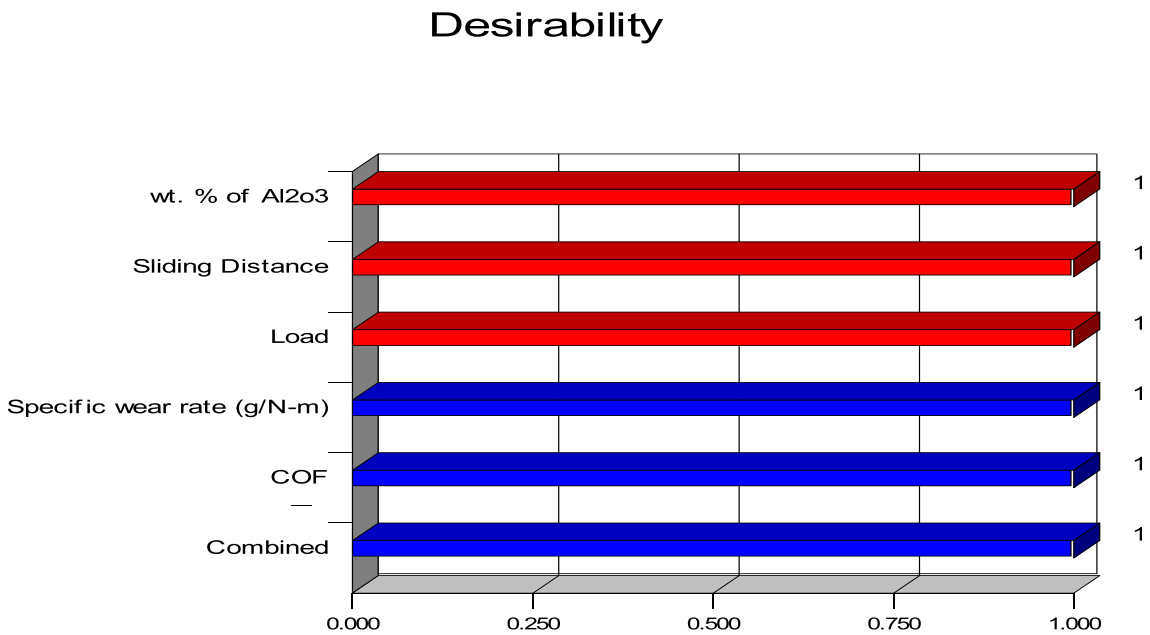

Fig. 11 Bar graph of desirability

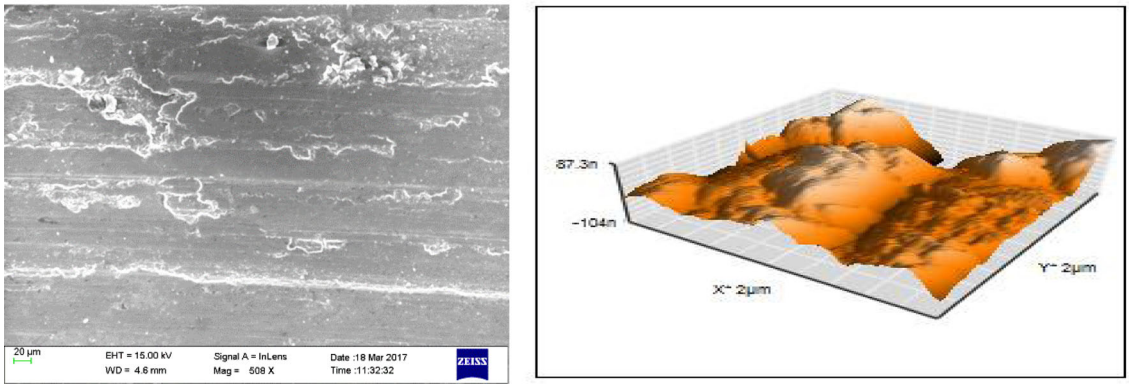

(a) (b)

Fig. 12 (a) SEM of Al-1.1Al_2O_3 worn surface (b) AFM of Al-1.1Al_2O_3 worn surface

dominating wear mechanisms of Al6061 are abrasive and adhesive wear.

Figure 7(b) shows the worn surface of Al-0.8Al_2O_3 nanocomposite at the applied load of 20 N. The SEM image shows parallel and less deep grooves due to abrasive wear. Figure 7(c) shows the worn surface of Al-0.8Al_2O_3 nanocomposite at the applied load of 40 N. It is observed that deep craters are formed on the nanocomposite worn surface which indicates that abrasive wear is dominant at high load. The worn surfaces of Al6061–0.8Al_2O_3 nanocomposite possess less plastic deformation when comparing to the wear surface of Al6061. From Fig. 7(d) and Fig. 7(e), it is observed that the wear surface appears more rough compared to Fig. 7(b) and Fig. 7(c). The most important factor is the presence of hard Al_2O_3 particles in the soft Al6061, which prevent the Al6061 from sliding wear and strengthen the Al6061. Moreover, these Al_2O_3 particles restrict the dispersion and cutting of the disc in to nanocomposite surface, thereby preventing delamination. In addition, the wear debris formed during dry sliding gets oxidized and forms a protective layer called mechanically mixed layer (MML) on the surface of nanocomposites. The worn surface of 0.8Al_2O_3 nanocomposite appears smooth, compared to Al6061 matrix alloy. The MML layer findings are consistent with Mosleh-Shirazi and Akhlaghi [4].

Figure 8 shows the AFM images of worn surfaces of (a) Al6061 D-2000 m L-40 N (b) Al-0.8Al_2O_3 D-3000 m L-20 N (c) Al-0.8Al_2O_3 D-3000 m L-40 N (d) Al-1.6Al_2O_3 D-3000 m L-20 N and (e) Al-1.6Al_2O_3 D-3000 m L-40 N (*L* load, *D* sliding distance). The results of AFM analysis match with wear examinations and the above said morphologies of worn surfaces. The AFM image of Al-0.8Al_2O_3 D-3000 m L-40 N exhibits relatively smooth surface after wear compared to matrix alloy. The worn surface of Al6061 indicates rough surface compared to nanocomposites.

4.5 EDS of wear worn surfaces

Figure 9(a–c) indicates the EDS of worn surface of alloy, nanocomposite after wear test under 40 N load. Figure 9(a) shows the EDS of the worn surface of alloy. It majorly contains aluminum which reveals that the alloy wear was high compared to the disc surface. The MML layer formation owing to the oxidation of iron and aluminum debris of nanocomposite is confirmed by the EDS analysis of Al6061–0.8Al_2O_3 nanocomposite, and Al6061–1.6Al_2O_3 nanocomposite was shown in Fig. 9(b) and Fig. 9(c). The hard MML lowers the SWR of the nanocomposite compared to Al6061 alloy [4].

4.6 Multiresponse optimization of Al6061-Al_2O_3 nanocomposite

It is important to identify the optimum parameters for any process. It is difficult to select the optimum condition for SWR and COF of Al6061-Al_2O_3 nanocomposite during dry sliding since it involves lots of process variables. Multiresponse tribological parameters are optimized using grey relational analysis, artificial neural networks with genetic algorithms, Taguchi's method, and desirability function approach. The desirability function approach is extensively used for optimization of multiresponse parameter in industry [24–27]. The value of desirability was evaluated using Design Expert software. RSM develops a set of data depending on input parameter to optimize the SWR and COF. The aim of optimization is to find the input parameters which minimize SWR and COF.

The various process parameters, its goal, upper and lower limit, and its optimum value of input parameters (load, distance, % of Al_2O_3) and output parameters (SWR and COF) are listed in Table 1. Out of various sets of input conditions, the one with highest desirability is chosen as optimum condition, and it is shown in Figs. 10 and 11. A dot on each ramp

indicates response prediction for that parameter. The overall desirability function of SWR and COF is shown in the bar graph of desirability. The range of desirability value is from 0 to 1. When the desirability value is close to 1, it indicates the closeness of the target. The set of parameters for optimization is as follows: Al_2O_3–1.1 wt.%; load-34 N and sliding distance-2931 m; with specific wear rate 1.06 g/N-m; and coefficient of friction, 0.305.

4.7 SEM and AFM image for optimization confirmation

The SEM and AFM analysis of the worn surface of Al6061–1.1Al_2O_3 at optimum condition is used to check the accuracy of the model. Figure 12(a) shows the worn surface at optimum conditions: load, 34 N, and sliding distance, 2931 m. It is observed that only small scratches are seen at few places of the worn surface, which is an indication of low SWR. It confirms the accuracy of the model. Figure 12(b) shows the 3D AFM image of the Al-Al_2O_3 nanocomposite. The height of the groove indicates the roughness of the surface. The lower the height, the lower will be the surface roughness. It is clear from the AFM image that at the optimum % of Al_2O_3 particles in the nanocomposite, there is decrease in groove height indicating the smoothness of the worn surface.

5 Conclusion

Aluminum metal matrix composite reinforced with Al_2O_3 nanoparticles was fabricated effectively employing ultrasonic cavitation-based solidification process.

The dry sliding wear of Al-Al_2O_3 nanocomposites were successfully carried out using Box-Behnken design of experiments of RSM by conducting 17 experiments for three factors at three levels.

The influence of process parameters on SWR and COF of Al-Al_2O_3 nanocomposites was investigated. A mathematical model was developed to predict the SWR and COF of Al-Al_2O_3 nanocomposites incorporating the effects of % reinforcement Al_2O_3, applied load, and sliding distance. The predicted values match the experimental values reasonably well with R^2 of SWR and COF.

ANOVA was used to check the adequacy of the model. The test results show minimum deviation between actual value and predicted value which confirms the accuracy of the developed model. The SWR and COF are significantly influenced by % Al_2O_3 followed by load and sliding distance.

The parameters were optimized using desirability-based multiresponse optimization technique to minimize the SWR and COF. The optimum parameters of combination setting for Al-Al_2O_3 nanocomposites obtained are Al_2O_3 of 1.1 wt.%, load of 34 N, and sliding distance of 2931 *m* for minimizing SWR and COF.

The AFM image of Al6061–1.1Al_2O_3 nanocomposite at optimized condition confirms the improvement in the wear surface smoothness of the nanocomposite compared to Al6061.

Nano-Al_2O_3 reinforced composites exhibited improved performance due to the formation of mechanically mixed layer (MML) at higher levels.

Compliance with ethical standards

Ethical statement The ethical standards were respected. The paper is written and submitted following the rules of good scientific practice.

Conflict of interest The authors declare they have no conflict of interest.

References

1. Anand Partheeban CM, Rajendran M, Vettivel SC, Suresh S, Moorthi NSV (2015) Mechanical behavior and failure analysis using online acoustic emission on nano-graphite reinforced Al6061–10TiB2 hybrid composite using powder metallurgy. Mater Sci Eng A 632:1–13
2. Miracle DB (2005) Metal matrix composites - from science to technological significance. Compos Sci Technol 65:2526–2540
3. Khorasani S, Heshmati-Manesh S, Abdizadeh H (2015) Improvement of mechanical properties in aluminum/CNTs nanocomposites by addition of mechanically activated graphite. Composites Part B 68:177–183
4. Mosleh-shirazi S, Akhlaghi F (2016) Wear behaviour of al 5252 alloy reinforced with micrometric and nanometric SiC particles. Tribol Int 102:28–37
5. Mosleh-Shirazi S, Akhlaghi F, Li DY (2016) Effect of graphite content on the wear behavior of Al/2SiC/gr hybrid nanocomposites respectively in the ambient environment and an acidic solution. Tribol Int 103:620–628
6. Manivannan I, Ranganathan S, Gopalakannan S, Suresh S, Nagakarthigan K (2017) Jubendradass R, Tribological and surface behavior of silicon carbide reinforced aluminum matrix nanocomposite. Surfaces and Interfaces 8:127–136
7. Sajjadi SA, Ezatpour HR, Beygi H (2011) Microstructure and mechanical properties of Al–Al2O3 micro and nano composites fabricated by stir casting. Mater Sci Eng A 528:8765–8771
8. Nie KB, Wang XJ, Wu K, Hu XS, Zheng MY (2012) Development of SiCp/AZ91 magnesium matrix nanocomposites using ultrasonic vibration. Mater Sci Eng A 540:123–129
9. Cao G, Choi H, Konishi H, Kou S, Lakes R, Li X (2008) Mg-6Zn/1.5SiC nanocomposites fabricated by ultrasonic cavitation based solidification processing. J Mater Sci 43:5521–5526
10. Manivannan I, Ranganathan S, Gopalakannan S, Suresh S (2018) Mechanical properties and tribological behavior of Al6061–SiC–Gr self-lubricating hybrid nanocomposites. Trans Indian Inst Metals 71(8):1897–1911
11. Sameezadeh M, Emamy M, Farhangi H (2011) Effects of particulate reinforcement and heat treatment on the hardness and wear properties of AA 2024-MoSi2 nanocomposites. Mater Des 32:2157–2164
12. MohammadSharifi E, Karimzadeh F, Enayati MH (2011) Fabrication and evaluation of mechanical and tribological

properties of boron carbide reinforced aluminum matrix nanocomposites. Mater Des 32:3263–3271
13. Ravindran P, Manisekar K, Vinoth Kumar S, Rathika P (2013) Investigation of microstructure and mechanical properties of aluminum hybrid nano-composites with the additions of solid lubricant. Mater Des 51:448–456
14. Suresh S, Moorthi NSV, Vettivel SC, Selvakumar N, Jinu GR (2014) Effect of graphite addition on mechanical behavior of Al6061/TiB2 hybrid composite using acoustic emission. Mater Sci Eng A 612:16–27
15. Wang XJ, Wang NZ, Wang LY, Hu XS, Wu K, Wang YQ, Huang YD (2014) Processing, microstructure and mechanical properties of micro-SiC particles reinforced magnesium matrix composites fabricated by stir casting assisted by ultrasonic treatment processing. Mater Des 57:638–645
16. Ezatpour HR, Torabiparizi M, Sajjadi SA (2015) Optimum selection of A356/Al2O3 nano/microcomposites fabricated with different conditions based on mathematical method. Proc IMechE Part L: J Materials: Design and Applications 0(0):1–9
17. Kumar S, Balasubramanian V (2008) Developing a mathematical model to evaluate wear rate of AA7075/SiCp powder metallurgy composites. Wear 264:1026–1034
18. Basavarajappa S, Chandramohan G, Subramanian R, Chandrasekar A (2006) Dry sliding wear behavior of Al2219/SiC metal matrix composites. Materals Science 24:357–366
19. Sahin Y (2007) Tribological behaviour of metal matrix and its composite. Mater Des 28:1348–1352
20. Suresha S, Sridhara BK (2010) Effect of addition of graphite particulates on the wear behaviour in aluminium–silicon carbide–graphite composites. Mater Des 31:1804–1812
21. Bayhan M, Onel K (2010) Optimization of reinforcement content and sliding distance for AlSi7Mg/SiCp composites using response surface methodology. Mater Des 31:3015–3022
22. Vettivel SC, Selvakumar N, Narayanasamy R, Leema N (2013) Numerical modeling prediction of cu-W nano powder composite in dry sliding wear condition using response surface methodology. Mater Des 50:977–996
23. Rajeev VR, Dwivedi DK, Jain SC (2010) Dry reciprocating wear of Al–Si–SiCp composites a statistical analysis. Tribol Int 43:1532–1541
24. Chiang KT (2008) Modeling and analysis of the effects of machining parameters on the performance characteristics in the EDM process of Al_2O_3+TiC mixed ceramic. Int J Adv Manuf Technol 37: 523–533
25. Ravi Kumar K, Sreebalaji VS (2015) Desirability based multiobjective optimization of abrasive wear and frictional behaviour of aluminium (Al/3.25Cu/8.5Si)/fly ash composites. Tribology - Materials, Surfaces & Interfaces 9:128–136
26. Ranganathan S, Senthilvelan T, Sriram S (2010) Evaluation of machining parameters of hot turning of stainless steel (type 316) by applying ANN and RSM. Mater Manuf Process 25(10):1131–1141
27. Gopalakannan S, Senthilvelan T (2013) Application of response surface method on machining of Al–SiC nano-composites. Measurement 46:2705–2715